

# Getting to the Point: Why Pointing Improves LVLMs

Simone Alghisi<sup>1</sup>, Massimo Rizzoli<sup>1</sup>, Seyed Mahed Mousavi<sup>1</sup>, and Giuseppe Riccardi<sup>1</sup>

Signals and Interactive Systems Lab, University of Trento, Povo TN 38123, IT  
{s.alghisi,massimo.rizzoli,giuseppe.riccardi}@unitn.it

**Abstract.** Pointing increases the accuracy and explainability of Large Vision-Language Models (LVLMs) by modeling grounding and reasoning as explicit sequential steps. The model grounds the objects mentioned in the natural-language query by predicting their coordinates, and then generates an answer conditioned on these points. While pointing has been shown to increase LVLMs’ accuracy, it is unclear which mechanism supports these gains and its relevance in cognitive tasks. In addition, the reliability of the intermediate points remains understudied, limiting their use as visual explanations. In this work, we study the role of pointing in a cognitive task: zero-shot counting from a visual scene. We fine-tune state-of-the-art LVLMs following two approaches: *Direct Counting*, where models only predict the total number of objects, and *Point-then-Count*, where LVLMs generate the target objects’ coordinates followed by their count. The results show that Point-then-Count achieves higher out-of-distribution generalization, suggesting that coordinates help LVLMs learn skills rather than overfitting on narrow tasks. Although predicted points are accurately grounded in the image in over 89% of cases (as measured by F1), performance varies across image regions, revealing spatial biases. Finally, mechanistic analyses show that gains in counting arise from the spatial information encoded in the coordinates<sup>1</sup>.

**Keywords:** Large Vision-Language Models · Pointing · Counting

## 1 Introduction

Large Vision–Language Models (LVLMs) combine a vision encoder with a Large Language Model (LLM), using natural language as an interface for solving different tasks within visual inputs (e.g., images). This paradigm has achieved strong results on several multimodal tasks, such as visual question answering, image captioning, and optical character recognition [5, 7, 13, 39]. However, prior work has shown that LVLm performance often degrades on more complex cognitive tasks that require spatial [20, 35], temporal [33], and counting [3, 14, 37] capabilities. Moreover, while some tasks require explicit visual evidence (e.g., grounded image captioning), in other settings LVLMs do not ground their answer in the image [50], making it difficult for humans to interpret.

<sup>1</sup> To support reproducibility, we release code, data, and model checkpoints on GitHub.

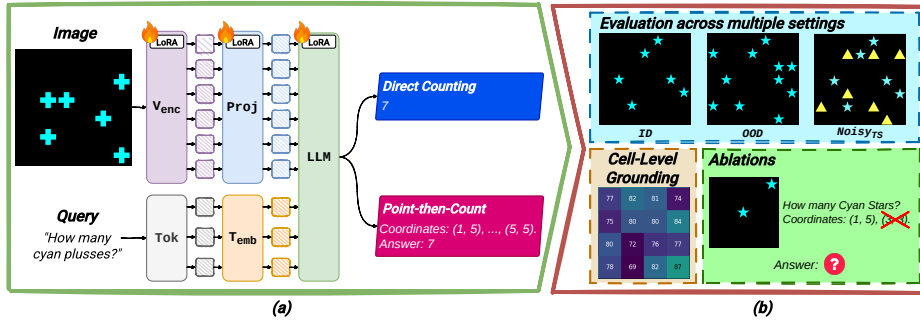


**Fig. 1:** Using counting as a case study, we (a) fine-tune four state-of-the-art LVLMs under two approaches, *Direct Counting* and *Point-then-Count* (PtC); (b) compare these approaches across settings. For PtC models, we assess whether predicted coordinates are grounded in the image and perform ablation studies to quantify their contribution.

To improve the accuracy and explainability of LVLMs, pointing-based methods [13] have recently proposed breaking complex tasks into two explicit sequential steps. Given a natural-language query about the objects in an image, the model first grounds the objects mentioned in the query by predicting their 2D coordinates in the image. Then, it generates an answer to the query, conditioned on these grounded coordinates. Recent studies have shown that pointing can improve final-task accuracy in counting [10, 13], spatial reasoning [45], robotic affordance prediction [48], and document understanding [28]. However, several key questions remain unresolved: i) Does pointing encourage learning skills (e.g., counting) rather than narrow tasks (e.g., counting in a fixed range or in the presence of distractors); ii) Are coordinates grounded in the visual input and therefore viable as explanations; and iii) What mechanism makes pointing improve performance? Addressing these questions is crucial for developing models capable of learning skills and producing outputs that are reliable and interpretable.

In this work, we study the role of pointing in zero-shot counting from a visual scene [3, 11, 49], a cognitive task that serves as a controlled benchmark for multi-step reasoning. We decompose counting into a two-step process: 1) grounding all target instances in the image that satisfy a natural language query, and 2) aggregating this information to return the number of target objects. This makes counting an ideal testbed for studying pointing, as the task naturally separates target grounding from subsequent aggregation. We present a visual overview of our approach in Fig. 1. We fine-tune four state-of-the-art LVLMs to count based on two different approaches: *Direct Counting* (DC), where models only predict the total number of objects, and *Point-then-Count* (PtC) [13], where LVLMs generate the target objects’ coordinates, followed by their count. To understand which training approach better supports skill learning, we evaluate LVLMs’ Out-of-Distribution (OOD) generalization under different scenarios, including images containing more targets and distractors than were observed during fine-tuning. For PtC models, we also study whether objects’ coordinates can serve as suitable

visual explanations by assessing how grounded these coordinates are in the image and their contributions towards the final prediction. Finally, to mitigate data contamination, reduce exploitable correlations during testing, and perform fine-grained analyses, we evaluate LVLMS by generating unseen synthetic datasets, balanced across object categories, labels, and spatial configurations.

We frame our work around three research questions:

1. **Does pointing encourage skill learning?** Using counting as a case study, we fine-tune four state-of-the-art LVLMS under two approaches, *DC* and *PtC*, and evaluate their performance across multiple settings. We find that point supervision improves performance in unseen scenario with more target objects than those observed during fine-tuning. When increasing the number of distractors, PtC still achieves the best overall performance, but some models benefit more from DC, suggesting that pre-training data and model scale may help generalize to higher distractor counts.
2. **Can Coordinates serve as valid and accurate visual explanations?** By comparing predicted coordinates with ground-truth annotations, we show that these points are grounded in more than 89% of cases. However, grounding performance for some models is not uniform across the image, hinting at potential pre-training biases or limitations in the attention mechanism.
3. **Why pointing improves performance?** When we replace each coordinate with an irrelevant token, no model achieves the same OOD generalization performance, underscoring the importance of spatial information for generalization. Further ablations reveal that PtC models mostly rely on coordinates to compute the total number of objects, disregarding the visual modality.

Our findings show that incorporating pointing as an intermediate task changes what LVLMS learn: models trained to generate grounded coordinates learn a more general counting procedure and expose intermediate evidence that can be verified. At the same time, the remaining failure modes indicate substantial room for improvement, motivating training paradigms that explicitly decompose perception and reasoning to better support transferable skill learning, stronger OOD robustness, and more interpretable outputs.

## 2 Literature Review

**Decomposing complex cognitive tasks** into intermediate sub-tasks facilitates learning in humans and animals [22]. In deep learning, providing intermediate sub-task outputs as additional supervision has been shown to benefit sequence-to-sequence models [41] in several language tasks such as solving math word problems [40], predicting code execution [29], and performing symbolic manipulation [36, 51]. Analogously, decomposition has been adopted in the vision-language domain to separate *perception* from *reasoning* [6, 46]. In this context, pointing [13] has been proposed as an intermediate subtask for LVLMS: instead of answering directly based on the image, the models first predict coordinates for the query-relevant objects and then condition subsequent generation on these

grounded cues. This approach has proven effective in counting [13], document understanding [28], spatial reasoning [45] and visual question answering [27]. However, prior work indicates that most LVLMs produce poorly aligned or unsupported intermediate groundings [42, 50]. Analyses show that these intermediate steps can contain factual errors, motivating evaluation protocols that assess the intermediate evidence itself rather than only task accuracy [43]. Although datasets with intermediate grounding annotations exist [23, 42], they are typically not constructed to localize *where* grounding breaks down within the image and may suffer from position biases (e.g., target object frequently appearing in the center [21]). To address this, we evaluate the grounding accuracy of LVLMs using datasets with a uniform spatial distribution of objects, which allows us to quantify their performance across image regions and diagnose spatial biases.

**Counting** requires a model to predict the total number of target objects in an image. While early work focused on counting fixed target objects [24, 25, 44] (e.g., people or cells), recent approaches generalize across classes by specifying the target in a few-shot [15, 17, 34, 47] (i.e., via visual exemplars) or zero-shot manner [9, 12, 18, 26, 30] (i.e., using a natural-language query). In zero-shot settings, contrastive vision-language models (e.g., CLIP [32]) are typically used as pipeline components to extract relevant visual and textual information [4, 31]; downstream modules then use this to localize, segment, or produce density maps for the target objects. In contrast, LVLMs are often (pre-)trained on multiple counting benchmarks [1, 8, 13], allowing them to count in an end-to-end manner. Although DC can eliminate the need for training additional task-specific modules, recent work shows that LVLMs can struggle even with small counts [3, 33] (e.g., up to ten), suggesting limited generalization beyond the count range seen during (pre-)training. PtC methods alleviate this by providing coordinates as intermediate supervision [13], yielding higher accuracy. Building on this line of work, we study the role of coordinates in zero-shot counting by comparing DC against a PtC approach. Unlike prior studies that primarily emphasize accuracy [7, 10, 13], our work focuses on explaining why coordinates help and what is the mechanism behind these gains.

### 3 Experimental Setting

We study the role of pointing-based methods in zero-shot counting on four state-of-the-art LVLMs. To mitigate data contamination, remove potential biases that models may exploit during testing, and perform a fine-grained analysis, we leverage the CIVET framework [35] to generate unseen synthetic datasets, balanced in terms of object type, position, and labels. We fine-tune each model following two approaches, DC and PtC, and test them on multiple scenarios to understand which method achieves better performance and why.

#### 3.1 Task: Zero-Shot Counting

We assess the counting capabilities of LVLMs in a zero-shot setting [8, 9, 13, 49]. The task requires determining the number of instances of a target object in an

image. In zero-shot counting, the target object is specified via a natural-language query, allowing users to include additional attributes. Formally, given:

- a model  $\mathcal{M}$ , capable of processing an image  $\mathcal{I}$  and a query  $q$  in natural language;
- an image  $\mathcal{I} \in \mathbb{R}^{H \times W \times C}$  with height  $H$ , width  $W$ , and  $C$  channels depicting some objects;
- a query  $q$  in natural language that specifies the **class** and (optionally) the attributes of the target object [3] (e.g., *How many blue stars are there?*).

we assess the counting capabilities of  $\mathcal{M}$  by comparing the generated answer  $\hat{y} = \mathcal{M}(\mathcal{I}, q)$  with  $y$ , where  $y \in \mathbb{N}_0$  corresponds to the number of targets objects in  $\mathcal{I}$  that match the class and attributes specified in  $q$ . To ensure  $\hat{y}$  follows our evaluation format, we employ a regex to remove any additional tokens (e.g., “The answer is . . .”, or “Answer: . . .”) and match the first valid answer. Further details are provided in the Supplementary Material.

### 3.2 Data

Existing datasets are often heavily imbalanced, both in terms of object classes [3] (e.g., “person” frequently dominating the distribution) and count [2] (small numbers occur far more often than larger ones). Most exhibit strong positional bias, with targets frequently appearing in the center [21], thereby limiting our understanding of their grounding capabilities. Curated subsets [8, 13] are often small and span only a narrow range, making them unsuitable to test OOD generalization. Finally, widely used real [1] and synthetic [19] datasets may have been included in the training data of some models, raising the risk of contamination.

We addressed these issues by generating tailored synthetic datasets with the CIVET framework [35], which provides fine-grained control over image content, allowing us to specify the class, attributes, and position of each object. Leveraging such control, we construct multiple datasets, ensuring exhaustive coverage in terms of object types and position, and uniform label distribution. For each dataset, we define a sample as a tuple  $(\mathcal{I}, q, \mathcal{C}, y)$ , where:

- $\mathcal{I}$  is an image, which we subdivide into an  $N \times M$  grid, where objects can be placed within each cell;
- $q$  is a natural-language query specifying the class and attributes of the target object;
- $\mathcal{C} = \{(n, m) \mid 0 \leq n < N, 0 \leq m < M\}$  is the set of grid coordinates  $(n, m)$  of all target objects in  $\mathcal{I}$ ;
- $y$  is the number of target objects contained in  $\mathcal{I}$  and corresponds to the cardinality of  $\mathcal{C}$  (i.e.,  $y = |\mathcal{C}|$ )

Having a grid-based representation gives us exact coordinates for each target object and control over the spatial layout. This makes the dataset ideal for training PtC models and for evaluating grounding without annotation errors.

For our experiments, we set  $N = M = 9$ . Following prior work [3], we mitigate the effect of external confounding factors by considering images with a uniform

black background, reducing the chance that irrelevant elements are mistaken for targets, and by placing objects in distinct cells to avoid occlusions. To ensure that the proposed setting does not induce a severe distribution shift, we run a preliminary experiment to assess the performance of LVLMs on the generated images (reported in the Supplementary Material). Results show that the models achieve more than 65% accuracy in this controlled setting, with Molmo achieving near-perfect accuracy, indicating that our protocol is compatible with the models’ (pre-)training distribution. Extending our evaluation to richer backgrounds and occlusions is left as future work.

Each query  $q$  is generated from a fixed template by substituting the target object class and attributes. Additional details on dataset construction are provided in the Supplementary Material.

**Training Data** We construct two balanced datasets to fine-tune LVLMs to count from one to nine. We focus on this range as prior work has shown that LVLMs exhibit limited counting ability even for small numerosities [2, 3], and existing curated benchmarks adopt a similar scope with the same number of labels [8, 13] (e.g., Pixmo-Count and CountBenchQA focus on the range [2, 10]). To avoid overfitting on a specific class-attribute combination, we consider 10 different target objects: six colored plusses (i.e., *red*, *green*, *blue*, *cyan*, *magenta*, *yellow*) and four white shapes (i.e., *circle*, *square*, *star*, *triangle*). We then generate two training settings:

- **Base.** We consider images containing only target objects to assess whether LVLMs can learn counting in a simplified setting, without confounders (e.g., occlusions or irrelevant objects). This design reduces ambiguity, ensuring that model errors can be attributed to counting failures rather than confusion between targets and irrelevant objects. To obtain a uniform label distribution, we generate 81 unique samples (i.e., with a different spatial configuration of objects) for each count in the range [1, 9]. Repeating this for all 10 target objects yields  $7,290^2$  samples in total (4,860/2,430 for training/validation).
- **Noisy<sub>TR</sub>.** Since real-world images often contain irrelevant objects that increase scene complexity, we create a second dataset in which each image includes up to three distractors. Starting from each image  $\mathcal{I}$  in the **Base** set, we add  $d \in \{1, 2, 3\}$  distractors to randomly selected empty cells. Each distractor is sampled uniformly from the set of non-target objects. To avoid introducing potential reasoning shortcuts, we enforce a uniform distribution over both the number and types of distractors. Since the resulting dataset matches the **Base** set in size (i.e., 7,290 samples), it allows us to isolate the effect of increased scene complexity on LVLMs’ learning.

**Evaluation Data** We construct three balanced datasets to test each approach under different evaluation settings and provide a visual overview in Fig. 1:

- **ID.** We construct an in-distribution (ID) test set following the same procedure as the **Base** setting, while varying class-attribute combinations and

<sup>2</sup> Computed as  $9 \text{ labels} \times 10 \text{ target objects} \times 81 \text{ unique spatial configurations}$

- spatial layouts to reduce overlap with training samples. Specifically, we consider the combinations of 4 classes (i.e., *square, circle, triangle, star*) and 6 colors (i.e., *red, green, blue, cyan, magenta, yellow*), for a total of 24 different target objects. The resulting dataset contains 17,496 samples and preserves the same uniform label distribution over the count range as the **Base** setting.
- **OOD**. To understand which approach leads to better OOD generalization in counting, we construct a test set with images depicting from 10 to 18 objects. We generate this dataset using the same target objects as in the **ID** setting, allowing us to isolate generalization to higher counts from changes in object categories and visual attributes. The resulting dataset contains 17,496 samples, with images containing at most twice the number of target objects seen during training.
  - **Noisy<sub>TS</sub>**. We construct a dataset to understand which counting approach is more robust to distractors. To isolate the effect of distractors, we build the test set by adding irrelevant objects to the images used in the **ID** setting while keeping the target count and positions fixed. Since exhaustively evaluating all target-distractor pairs is computationally infeasible, we fix the target to *blue star*, which achieves the highest counting accuracy in the **ID** setting (full analysis available in the Supplementary). This choice reduces computational cost and limits failures due to target identification. As distractors, we consider the remaining 23 class-attribute combinations, allowing us to marginalize over distractor types. To analyze the effect of distractor quantity, we subdivide the dataset into nine segments, where segment  $d \in \{1, \dots, 9\}$  contains images with exactly  $d$  distractors. To marginalize over distractor placement, we instantiate three distinct spatial configurations per image by placing the  $d$  distractors in different empty cells. Each segment contains  $50,301^3$  samples, for a total of 452,709 samples.

### 3.3 Approach

We fine-tune each LVLMS to count under two approaches, **DC** and **PtC**, and compare their performance on unseen scenarios to understand which method generalizes better and why. Following the notation introduced in Secs. 3.1 and 3.2, each model  $\mathcal{M}$  takes as input an image  $\mathcal{I}$  and a natural-language query  $q$  specifying the target class and attributes. In **DC**, we optimize  $\mathcal{M}$  to map the input pair  $(\mathcal{I}, q)$  directly to the target count  $y$ . In **PtC** we fine-tune  $\mathcal{M}$  to first predict the coordinates  $\mathcal{C}$  of the target objects based on  $(\mathcal{I}, q)$ , and subsequently generate the target count  $y$ . Specifically, we prepend  $\mathcal{C}$  to the target count  $y$ , and optimize the model’s parameters such that  $\mathcal{M}(\mathcal{I}, q) = \text{“Coordinates: } (n_1, m_1), (n_2, m_2), \dots, (n_y, m_y). \text{ Answer: } y\text{”}$ . We sort the coordinates in a fixed left-to-right, top-to-bottom order, which was shown to outperform a random ordering [13].

To ensure that differences in performance can be attributed to the learning objective, we fine-tune all LVLMS using the same training protocol. For both

<sup>3</sup> Computed as  $9 \text{ labels} \times 1 \text{ target object} \times 81 \text{ target spatial configurations} \times 23 \text{ distractor types} \times 3 \text{ distractor spatial configurations}$ .

approaches, models are optimized with the standard next-token prediction objective [13] using LoRA [16]. At inference time, we generate the answers with greedy decoding, using each LVLm’s default stopping criterion. Additional details about training, inference, and hardware can be found in the Supplementary Material.

### 3.4 Models

To understand whether our findings generalize across LVLms with different architectural and image pre-processing choices, we evaluate representative state-of-the-art models: Qwen2.5-VL 7B [7], LLaVA-OneVision-1.5 8B [5], and InternVL3.5 8B [39]. In addition, we include Qwen2.5-VL 3B to study the effect of LLM scaling. LVLms combine a vision encoder with an LLM (i.e., a text decoder) to perform vision-language tasks, but differ in how visual features are integrated into the language model. Both LLaVA-OneVision and InternVL3.5 employ a learned projection layer to map the visual information extracted by the encoder into the LLM embedding space, while in Qwen2.5-VL the visual representation is passed directly to the decoder. Regarding image pre-processing, InternVL3.5 applies dynamic tiling, splitting each image into non-overlapping  $448 \times 448$  crops. In contrast, LLaVA-OneVision and Qwen2.5-VL support variable-resolution inputs, eliminating the need for explicit resizing or cropping. Additional details about the checkpoint used for each model can be found in the Supplementary.

## 4 Experiments

We fine-tune four state-of-the-art LVLms to count under two training approaches: DC and PtC. To evaluate which approach better supports skill acquisition, we compare their performance in an OOD scenario. We further examine whether predicted coordinates can serve as valid and accurate visual explanations, and conduct a mechanistic analysis to understand how pointing influences counting behavior. Because all datasets are balanced across object types and count labels, we report our results using accuracy. Unless stated otherwise, results are obtained by fine-tuning on the **Base** dataset.

### 4.1 Does Pointing Always Improve Performance?

Although pointing has been shown to improve LVLms’ counting accuracy [13], it is unknown whether point supervision always outperforms DC. Investigating this question is crucial in practical applications, as the additional computation time and resources required to generate the targets’ coordinates may outweigh modest accuracy gains. We address this by comparing DC and PtC under the ID setting, and analyze performance as a function of the number of target objects. The results reported in Fig. 2 show that, when evaluated using in-distribution data (i.e., on the same count range seen during training), LLaVA-OneVision and InternVL3.5 are mostly unaffected by the choice of the training approach. In

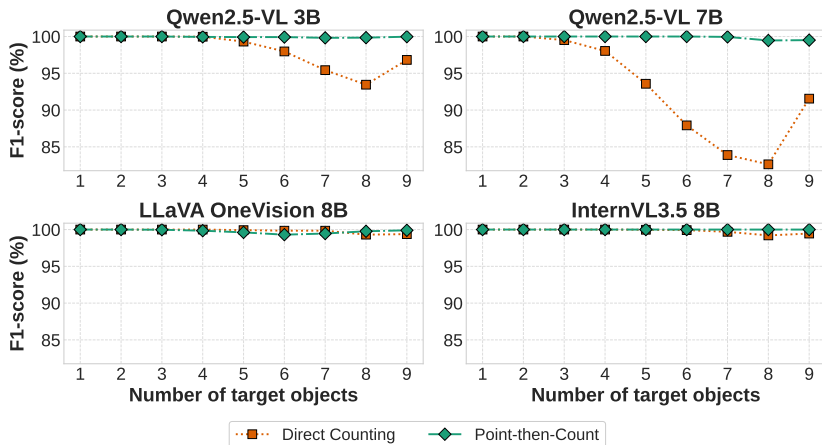


**Fig. 2:** F1-score as a function of the number of target objects under the ID setting for models fine-tuned with DC or PtC. While LLaVA-OneVision and InternVL3.5 show similar performance, Qwen2.5-VL models benefit more from point supervision, suggesting PtC as a more robust choice across object counts.

contrast, after fine-tuning for DC, the performance for both Qwen2.5-VL models degrades as the number of objects increases, with a clear drop when moving from 1 to 8 objects. Interestingly, despite fine-tuning on a balanced dataset (Sec. 3.2), performance increases for 9 objects. This non-monotonic pattern is not observed for PtC, where performance remains more stable across object counts.

Overall, our findings reveal that although DC and PtC perform comparably in-domain for some models, point supervision yields more stable behavior as object counts increase, making it a more reliable choice for robust counting.

## 4.2 Which Approach Encourages Skill Learning?

Understanding how models behave in unseen scenarios is particularly important for deployment, where the number of target objects may exceed what the model observed during training. In addition, investigating which approach leads to higher generalization is crucial for training, as collecting balanced real-world data for high object counts is almost unfeasible. To this end, we assess which approach encourages skill learning by measuring their performance in an OOD setting, using images containing from 10 to 18 objects (i.e., at most twice the targets seen during training). Results in Tab. 1a show that, except for Qwen2.5-VL 3B, models fine-tuned with PtC achieve higher accuracy, suggesting that pointing may teach a more robust counting strategy, capable of generalizing to higher object counts. However, the magnitude of these gains varies across models, potentially due to differences in architecture or pre-training data.

To get more insights about this variability, we conduct an analysis of the generated responses and provide additional details in Sec. 4.4. We find that

**Table 1:** Accuracy (%) of each model on the OOD setting. **(a)** reports DC and PtC accuracy using the model’s final prediction (i.e., the value after “Answer:”). **(b)** reports PtC accuracy computed from the number of predicted coordinates. Arrows ( $\uparrow$  /  $\downarrow$ ) indicate absolute increase or decrease with respect to the corresponding pre-trained model. Overall, computing the count from the number of predicted points yields the highest accuracy across models.

Model	DC	PtC	# Coordinates
<i>Qwen2.5-VL 3B</i>	31.66 ( $\uparrow$ 10.03)	19.52 ( $\downarrow$ 2.12)	81.65 ( $\uparrow$ 60.01)
<i>Qwen2.5-VL 7B</i>	31.88 ( $\uparrow$ 8.94)	46.54 ( $\uparrow$ 23.61)	94.78 ( $\uparrow$ 71.85)
<i>LLaVA-OneVision 8B</i>	31.06 ( $\uparrow$ 11.84)	72.38 ( $\uparrow$ 53.16)	92.11 ( $\uparrow$ 72.89)
<i>InternVL3.5 8B</i>	45.38 ( $\downarrow$ 0.97)	97.33 ( $\uparrow$ 50.99)	98.05 ( $\uparrow$ 51.70)

(a)
(b)

most models correctly ground the target objects but often predict an incorrect count. This inconsistency suggests that models may fail to associate the predicted coordinates with the correct numerical value. To test this hypothesis, we perform an additional experiment in which the final count is derived directly from the number of predicted coordinates (i.e., using a regex). The results in Tab. 1b confirm our hypothesis, showing that using the coordinates to count increases accuracy substantially, with 7B and 8B models exceeding 90%. Qwen2.5-VL 3B also exhibits a large improvement (surpassing 80%), but its performance remains below that of larger models, suggesting that model capacity may be important.

These results highlight point supervision as a key factor for generalization to higher object counts. Moreover, differing from prior work [13], we observe that using the predicted coordinates to count can be advantageous beyond the training distribution, as the model’s final answer is often inconsistent with the number of predicted points.

### 4.3 Does Point Supervision Improve Robustness to Distractors?

So far, we have only considered images containing target objects to ensure that these models were capable of counting in a controlled scenario. However, real-world scenes are usually characterized by visually similar objects that, despite being different from the target, may be erroneously included in the total count. Assessing the robustness to distractors is crucial for sensitive applications, where even subtle changes could significantly impact the results (e.g., counting specific white blood cells to identify leukemia [38]).

To understand which approach is more robust to distractors, we fine-tune the models on a modified set that includes images with up to three distractors (i.e., **Noisy<sub>TR</sub>**). We then evaluate their robustness on images containing up to nine distractors (i.e., **Noisy<sub>TS</sub>**) and report the results in Fig. 3. Our plots show that pre-trained models become less accurate as the number of distractors increases, suggesting that they miscount in the presence of distractors. The only exception is InternVL3.5, which seems to be equally affected by 1 or 9 distractors. Both DC

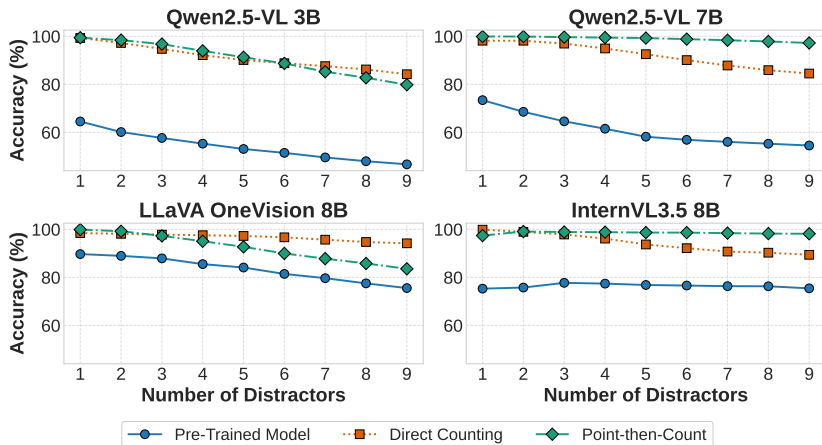


**Fig. 3:** Accuracy (%) as a function of the number of distractors after fine-tuning on  $\text{Noisy}_{\text{TR}}$  for DC or PtC. PtC maintains near-perfect accuracy for InternVL3.5 and Qwen2.5-VL 7B, while for Qwen2.5-VL 3B and LLaVA-OneVision PtC degrades faster than DC as distractors increase.

and PtC improve over the pre-trained models, but point supervision is particularly effective for InternVL3.5 and Qwen2.5-VL 7B, which maintain more stable results and achieve near-perfect accuracy even with nine distractors. For the remaining models, point supervision helps up to a moderate number of distractors, but degrades more quickly than DC once distractors become more numerous.

Overall, these results suggest that point supervision can yield more stable performance. However, generalization to a higher number of distractors depends on model architecture and/or (pre-)training data.

#### 4.4 Are Coordinates Valid and Accurate Visual Explanations?

While our results show that coordinates can improve LVLm accuracy, especially in the OOD setting, their usefulness as visual explanations depends on whether they are grounded in the image and consistent with the final answer. We therefore evaluate their reliability using three metrics: F1-score, which captures both missed targets and hallucinated points; exact match (EM), which assesses whether the entire set of coordinates is correct; and consistency (Cons.), which measures whether the number of coordinates matches the final count. Results in Tab. 2 show that coordinates are especially reliable in the ID setting, since it matches the training distribution. Consistency degrades in the OOD setting, indicating that the number of predicted coordinates does not match the models’ final count (as discussed in Sec. 4.2). Exact match reveals that, although some models achieve over 90% counting accuracy (Tab. 1b), coordinates are not always fully correct. For example, Qwen2.5-VL 7B reaches 94% accuracy but only 88% EM, indicating that in roughly 6% of cases at least one coordinate is wrong.

**Table 2:** Coordinate reliability (%) across three settings, reported using F1-score, exact match (EM), and consistency (Cons.). Results for `NoisyTS` are computed only on images containing 9 distractors.

Model	ID			OOD			Noisy <sub>TS</sub>		
	F1	EM	Cons.	F1	EM	Cons.	F1	EM	Cons.
<i>Qwen2.5-VL-3B</i>	99.91	99.59	100.00	94.52	76.07	20.56	93.59	69.76	99.56
<i>Qwen2.5-VL-7B</i>	99.89	99.55	100.00	98.59	88.05	48.79	99.19	95.77	99.75
<i>LLaVA OneVision 8B</i>	99.52	98.31	99.98	96.91	80.88	77.72	89.59	70.57	99.82
<i>InternVL3.5 8B</i>	100.00	100.00	100.00	99.89	98.06	99.27	99.84	99.05	98.51

Nevertheless, the F1-score remains high across all models, suggesting that errors affect only a small subset. Finally, on `NoisyTS`<sup>4</sup> results show that, despite each model being highly consistent, EM drops substantially for Qwen2.5-VL 3B and LLaVA-OneVision, indicating that most failures stem from localization errors.

Simply reporting the average performance may hide potential spatial biases: a reliable system should provide accurate results regardless of the object’s position in the image. Different from prior work, we conduct a fine-grained analysis and study whether coordinates are uniformly grounded across the image. We compute the F1-score for each cell of our 9×9 grid and report results in Fig. 4. Due to space constraints, we focus on the images with nine distractors (`NoisyTS`), as this corresponds to the most challenging setting in terms of F1-score (as shown in Tab. 2). Figures for the other settings, along with additional analyses, are provided in the Supplementary Material. Results reveal that LLaVA-OneVision exhibits the most pronounced spatial biases, with performance progressively decreasing from left to right. Qwen2.5-VL 3B shows a different trend and achieves a lower F1-score at the bottom and right edges. Qwen2.5-VL 7B exhibits a similar, yet less concerning, pattern, suggesting the possibility of a shared bias within this model family. The only exception is InternVL3.5, which maintains a near-uniform and perfect F1-Score across the image.

Our findings reveal that coordinates are grounded in the image in more than 89% of the cases (as measured by F1 score), supporting their use as potential visual explanations. However, some models exhibit spatial biases and reduced exact-match performance, particularly in noisy settings with irrelevant objects. Thus, even when most points are correct, errors can concentrate in specific regions and undermine the reliability of point-based explanations.

#### 4.5 Why does Pointing Improve Performance?

After showing that pointing improves LVLm counting accuracy and analyzing the reliability of the predicted coordinates, an important question remains: why does it help? Addressing this question is essential for understanding whether other tasks might also benefit from point supervision. To this end, we conduct

<sup>4</sup> We report results only for images with nine distractors, as this corresponds to the most challenging segment (see Fig. 3).

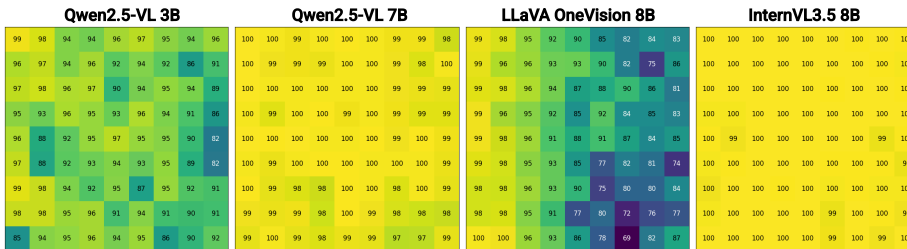


**Fig. 4:** Cell-level F1-score (%) for each model across our  $9 \times 9$  grid. Results are computed on images containing 9 distractors. LLaVA-OneVision shows a clear left-to-right performance drop, while Qwen2.5-VL models achieve a lower F1-score at the bottom and right edges. In contrast, InternVL3.5 maintains near-uniform performance across the image.

a series of ablations to study why pointing improves LVLMs’ counting accuracy, focusing on the OOD setting. We hypothesize that coordinates provide explicit spatial cues that help the model disambiguate among object instances. If this is the case, replacing coordinates with a location-agnostic token should remove the spatial signal and degrade performance. To test this, we fine-tune each model for PtC, but replace each coordinate with the token "X", and report results in Tab. 3a. Our results show that removing spatial information consistently reduces accuracy, indicating that spatial information is the key to improving LVLMs’ generalization to higher object counts. The largest drop occurs for Qwen2.5-VL 7B, which tends to repeatedly generate "X" tokens instead of producing meaningful outputs (despite achieving 97% on the ID setting, as reported in the Supplementary).

To better understand how models leverage coordinates when counting, we conduct two additional ablations. First, we assess the model’s reliance on coordinates by replacing  $\mathcal{I}$  with a black image while providing ground-truth coordinates  $\mathcal{C}$  as input. Second, we perform a leave-one-out ablation in which we remove one coordinate at a time and measure whether the model can recover the missing point. We perform our ablations on the ID setting, where models achieve the highest accuracy (Fig. 2) and consistency (Tab. 2), making it well-suited to study the contribution of coordinates on the model’s final count. Results in Tab. 3b reveal that removing the image has little to no effect ( $< 2\%$  drop) on performance, indicating that models generate the final count solely based on the coordinates, disregarding almost completely the visual modality. Ablating the coordinates leads to a significant drop in accuracy ( $> 81\%$ ), indicating that models are not capable of recovering when coordinate information is removed.

Our mechanistic analysis indicates that spatial information helps LVLMs to generalize to higher object counts, suggesting that adding a grounding step may benefit other vision-language tasks. Moreover, we find that models rely primarily on the textual coordinates to produce the final count, indicating that reasoning over a structured representation may be easier than using raw visual features.

**Table 3:** Accuracy (%) of each model on different ablations. **(a)** reports performance on the OOD setting after X Fine-Tuning, where we replace each coordinate with an "X" during PtC training. **(b)** reports accuracy on the ID setting when ablating the input image or the coordinates. Values in parentheses indicate absolute change with respect to the PtC baseline. Results highlight the importance of spatial information to improve generalization and the dominant role of the textual coordinate when counting.

Model	X Fine-Tuning	Ablate Image	Ablate Coordinates
<i>Qwen2.5-VL 3B</i>	21.15 (↓ 60.50)	98.72 (↓ 1.22)	7.81 (↓ 92.13)
<i>Qwen2.5-VL 7B</i>	3.36 (↓ 91.42)	100.00 (↑ 0.12)	14.24 (↓ 85.64)
<i>LLaVA-OneVision 8B</i>	16.33 (↓ 75.78)	98.77 (↓ 0.99)	6.11 (↓ 93.65)
<i>InternVL3.5 8B</i>	37.05 (↓ 61.00)	100.00 (= 0.00)	18.19 (↓ 81.81)

(a)
(b)

## 5 Discussion & Conclusion

We studied the role of pointing-based supervision for zero-shot counting by comparing Direct Counting (CT) with Point-then-Count (PtC) across multiple settings. Our results show that PtC achieves higher OOD generalization, especially in regimes with more objects, suggesting that intermediate grounding encourages skill learning. The generated coordinates are grounded in over 89% of cases, making them viable visual explanations. Ablations reveal that the spatial information in the coordinates is fundamental for generalizing to higher object counts. Moreover, PtC models primarily rely on the textual coordinates to count, disregarding the image content.

Despite these advantages, generating intermediate coordinates incurs additional computational cost, which grows with the number of target objects. Future work should therefore investigate more efficient grounding mechanisms to reduce inference overhead. We focused our analysis on open-source LVLMs up to 8B parameters, since proprietary models cannot be fine-tuned, and larger models exceed our computational resources. Regarding our data, although we used balanced synthetic datasets to remove confounding factors, validating these findings on natural images with clutter and occlusion remains essential. Nevertheless, prior work has already shown the benefits of point supervision in real-world settings, suggesting our conclusions may extend beyond the synthetic regime. Lastly, while our results indicate grounding provides useful spatial information for subsequent reasoning in counting, we hypothesize that other object-centric tasks may similarly benefit, based on previous studies on spatial reasoning, document understanding, and robotic affordance prediction. In the future, we plan to extend our results to more challenging scenarios, address the remaining limitations, and explore novel training strategies that better integrate grounding with visual reasoning.

## References

1. Acharya, M., Kafle, K., Kanan, C.: Tallyqa: Answering complex counting questions. In: Proceedings of the AAAI conference on artificial intelligence. pp. 8076–8084 (2019)
2. Al-Tahan, H., Garrido, Q., Balestriero, R., Bouchacourt, D., Hazirbas, C., Ibrahim, M.: Unibench: Visual reasoning requires rethinking vision-language beyond scaling. In: The 38th Conference on Neural Information Processing Systems Datasets and Benchmarks Track. pp. 82411–82437 (2024)
3. Alghisi, S., Roccabruna, G., Rizzoli, M., Mousavi, S.M., Riccardi, G.: [de|re] constructing vlms’ reasoning in counting. arXiv preprint arXiv:2510.19555 (2025)
4. Amini-Naieni, N., Han, T., Zisserman, A.: Countgd: Multi-modal open-world counting. In: Globerson, A., Mackey, L., Belgrave, D., Fan, A., Paquet, U., Tomczak, J., Zhang, C. (eds.) Advances in Neural Information Processing Systems. vol. 37, pp. 48810–48837. Curran Associates, Inc. (2024). <https://doi.org/10.52202/079017-1547>, [https://proceedings.neurips.cc/paper\\_files/paper/2024/file/57c56985d9afe89bf78a8264c91071aa-Paper-Conference.pdf](https://proceedings.neurips.cc/paper_files/paper/2024/file/57c56985d9afe89bf78a8264c91071aa-Paper-Conference.pdf)
5. An, X., Xie, Y., Yang, K., Zhang, W., Zhao, X., Cheng, Z., Wang, Y., Xu, S., Chen, C., Zhu, D., et al.: Llava-onevision-1.5: Fully open framework for democratized multimodal training. arXiv preprint arXiv:2509.23661 (2025)
6. Andreas, J., Rohrbach, M., Darrell, T., Klein, D.: Neural module networks. In: Proceedings of the IEEE Conference on Computer Vision and Pattern Recognition (CVPR) (June 2016)
7. Bai, S., Chen, K., Liu, X., Wang, J., Ge, W., Song, S., Dang, K., Wang, P., Wang, S., Tang, J., et al.: Qwen2. 5-vl technical report. arXiv preprint arXiv:2502.13923 (2025)
8. Beyer, L., Steiner, A., Pinto, A.S., Kolesnikov, A., Wang, X., Salz, D., Neumann, M., Alabdulmohsin, I., Tschannen, M., Bugliarello, E., et al.: Paligemma: A versatile 3b vlm for transfer. arXiv preprint arXiv:2407.07726 (2024)
9. Campbell, D., Rane, S., Giallanza, T., De Sabbata, C.N., Ghods, K., Joshi, A., Ku, A., Frankland, S., Griffiths, T., Cohen, J.D., et al.: Understanding the limits of vision language models through the lens of the binding problem. Advances in Neural Information Processing Systems **37**, 113436–113460 (2024)
10. Clark, C., Zhang, J., Ma, Z., Park, J.S., Salehi, M., Tripathi, R., Lee, S., Ren, Z., Kim, C.D., Yang, Y., et al.: Molmo2: Open weights and data for vision-language models with video understanding and grounding. arXiv preprint arXiv:2601.10611 (2026)
11. Dai, S., Liu, J., Cheung, N.M.: Referring expression counting. In: Proceedings of the IEEE/CVF Conference on Computer Vision and Pattern Recognition. pp. 16985–16995 (2024)
12. Dai, S., Liu, J., Cheung, N.M.: Referring expression counting. In: Proceedings of the IEEE/CVF Conference on Computer Vision and Pattern Recognition (CVPR). pp. 16985–16995 (June 2024)
13. Deitke, M., Clark, C., Lee, S., Tripathi, R., Yang, Y., Park, J.S., Salehi, M., Muenighoff, N., Lo, K., Soldaini, L., Lu, J., Anderson, T., Bransom, E., Ehsani, K., Ngo, H., Chen, Y., Patel, A., Yatskar, M., Callison-Burch, C., Head, A., Hendrix, R., Bastani, F., VanderBilt, E., Lambert, N., Chou, Y., Chheda, A., Sparks, J., Skjonsberg, S., Schmitz, M., Sarnat, A., Bischoff, B., Walsh, P., Newell, C., Wolters, P., Gupta, T., Zeng, K.H., Borchardt, J., Groeneveld, D., Nam, C., Lebrecht, S.,

- Wittlif, C., Schoenick, C., Michel, O., Krishna, R., Weihs, L., Smith, N.A., Hajishirzi, H., Girshick, R., Farhadi, A., Kembhavi, A.: Molmo and pixmo: Open weights and open data for state-of-the-art vision-language models. In: Proceedings of the IEEE/CVF Conference on Computer Vision and Pattern Recognition (CVPR). pp. 91–104 (June 2025)
14. Fu, C., Dai, Y., Luo, Y., Li, L., Ren, S., Zhang, R., Wang, Z., Zhou, C., Shen, Y., Zhang, M., Chen, P., Li, Y., Lin, S., Zhao, S., Li, K., Xu, T., Zheng, X., Chen, E., Shan, C., He, R., Sun, X.: Video-mme: The first-ever comprehensive evaluation benchmark of multi-modal llms in video analysis. In: Proceedings of the IEEE/CVF Conference on Computer Vision and Pattern Recognition (CVPR). pp. 24108–24118 (June 2025)
  15. He, J., Liu, B., Cao, F., Xu, J., Xiao, Y.: Few-shot object counting with dynamic similarity-aware in latent space. *IEEE Transactions on Geoscience and Remote Sensing* **62**, 1–14 (2024)
  16. Hu, E.J., yelong shen, Wallis, P., Allen-Zhu, Z., Li, Y., Wang, S., Wang, L., Chen, W.: LoRA: Low-rank adaptation of large language models. In: International Conference on Learning Representations (2022), <https://openreview.net/forum?id=nZeVKeeFYf9>
  17. Jeon, Y., Lee, S., Kim, J., Heo, J.P.: Mutually-aware feature learning for few-shot object counting. *Pattern Recognition* **161**, 111276 (2025). <https://doi.org/https://doi.org/10.1016/j.patcog.2024.111276>, <https://www.sciencedirect.com/science/article/pii/S0031320324010276>
  18. Jiang, R., Liu, L., Chen, C.: Clip-count: Towards text-guided zero-shot object counting. In: Proceedings of the 31st ACM International Conference on Multimedia. p. 4535–4545 (2023)
  19. Johnson, J., Hariharan, B., van der Maaten, L., Fei-Fei, L., Lawrence Zitnick, C., Girshick, R.: Clevr: A diagnostic dataset for compositional language and elementary visual reasoning. In: Proceedings of the IEEE Conference on Computer Vision and Pattern Recognition (CVPR) (2017)
  20. Kamath, A., Hessel, J., Chang, K.W.: What’s “up” with vision-language models? investigating their struggle with spatial reasoning. In: Proceedings of the 2023 Conference on Empirical Methods in Natural Language Processing. pp. 9161–9175 (2023)
  21. Kirillov, A., Mintun, E., Ravi, N., Mao, H., Rolland, C., Gustafson, L., Xiao, T., Whitehead, S., Berg, A.C., Lo, W.Y., et al.: Segment anything. In: Proceedings of the IEEE/CVF international conference on computer vision. pp. 4015–4026 (2023)
  22. Krueger, K.A., Dayan, P.: Flexible shaping: How learning in small steps helps. *Cognition* **110**(3), 380–394 (2009). <https://doi.org/https://doi.org/10.1016/j.cognition.2008.11.014>, <https://www.sciencedirect.com/science/article/pii/S0010027708002850>
  23. Lei, J., Yu, L., Berg, T., Bansal, M.: TVQA+: Spatio-temporal grounding for video question answering. In: Jurafsky, D., Chai, J., Schluter, N., Tetreault, J. (eds.) Proceedings of the 58th Annual Meeting of the Association for Computational Linguistics. pp. 8211–8225. Association for Computational Linguistics, Online (Jul 2020). <https://doi.org/10.18653/v1/2020.acl-main.730>, <https://aclanthology.org/2020.acl-main.730/>
  24. Liang, D., Xu, W., Bai, X.: An end-to-end transformer model for crowd localization. In: European Conference on Computer Vision. pp. 38–54 (2022)
  25. Lin, H., Ma, Z., Ji, R., Wang, Y., Hong, X.: Boosting crowd counting via multifaceted attention. In: Proceedings of the IEEE/CVF conference on computer vision and pattern recognition. pp. 19628–19637 (2022)

26. Liu, S., Zhang, P., Zhang, S., Ke, W.: Countse: Soft exemplar open-set object counting. In: Proceedings of the IEEE/CVF International Conference on Computer Vision (ICCV). pp. 21536–21546 (October 2025)
27. Man, Y., Huang, D.A., Liu, G., Sheng, S., Liu, S., Gui, L.Y., Kautz, J., Wang, Y.X., Yu, Z.: Argus: Vision-centric reasoning with grounded chain-of-thought. In: Proceedings of the IEEE/CVF Conference on Computer Vision and Pattern Recognition (CVPR). pp. 14268–14280 (June 2025)
28. Ni, M., Yang, Z., Li, L., Lin, C.C., Lin, K., Zuo, W., Wang, L.: Point-rft: Improving multimodal reasoning with visually grounded reinforcement finetuning. arXiv preprint arXiv:2505.19702 (2025)
29. Nye, M., Andreassen, A.J., Gur-Ari, G., Michalewski, H., Austin, J., Bieber, D., Dohan, D., Lewkowycz, A., Bosma, M., Luan, D., Sutton, C., Odena, A.: Show your work: Scratchpads for intermediate computation with language models (2022), <https://openreview.net/forum?id=iedYJm92o0a>
30. Paiss, R., Ephrat, A., Tov, O., Zada, S., Mosseri, I., Irani, M., Dekel, T.: Teaching clip to count to ten. In: Proceedings of the IEEE/CVF International Conference on Computer Vision (ICCV). pp. 3170–3180 (2023)
31. Qian, Y., Guo, Z., Deng, B., Lei, C.T., Zhao, S., Lau, C.P., Hong, X., Pound, M.P.: T2icount: Enhancing cross-modal understanding for zero-shot counting. In: Proceedings of the Computer Vision and Pattern Recognition Conference. pp. 25336–25345 (2025)
32. Radford, A., Kim, J.W., Hallacy, C., Ramesh, A., Goh, G., Agarwal, S., Sastry, G., Askell, A., Mishkin, P., Clark, J., Krueger, G., Sutskever, I.: Learning transferable visual models from natural language supervision. In: Proceedings of the 38th International Conference on Machine Learning. pp. 8748–8763 (2021)
33. Rahmanzadehgervi, P., Bolton, L., Taesiri, M.R., Nguyen, A.T.: Vision language models are blind. In: Proceedings of the Asian Conference on Computer Vision (ACCV). pp. 18–34 (December 2024)
34. Ranjan, V., Sharma, U., Nguyen, T., Hoai, M.: Learning to count everything. In: Proceedings of the IEEE/CVF Conference on Computer Vision and Pattern Recognition (CVPR). pp. 3394–3403 (June 2021)
35. Rizzoli, M., Alghisi, S., Khomyn, O., Roccabruna, G., Mousavi, S.M., Riccardi, G.: CIVET: Systematic evaluation of understanding in VLMs. In: Christodoulopoulos, C., Chakraborty, T., Rose, C., Peng, V. (eds.) Findings of the Association for Computational Linguistics: EMNLP 2025. pp. 4462–4480. Association for Computational Linguistics, Suzhou, China (Nov 2025). <https://doi.org/10.18653/v1/2025.findings-emnlp.239>, <https://aclanthology.org/2025.findings-emnlp.239/>
36. Sprague, Z.R., Yin, F., Rodriguez, J.D., Jiang, D., Wadhwa, M., Singhal, P., Zhao, X., Ye, X., Mahowald, K., Durrett, G.: To cot or not to cot? chain-of-thought helps mainly on math and symbolic reasoning. In: The Thirteenth International Conference on Learning Representations (2025), <https://openreview.net/forum?id=w6n1cS8Kkn>
37. Vo, A., Nguyen, K.N., Taesiri, M.R., Dang, V.T., Nguyen, A.T., Kim, D.: Vision language models are biased: Counting legs of an animal is surprisingly hard. In: 2nd AI for Math Workshop @ ICML 2025 (2025), <https://openreview.net/forum?id=O2xoCaU6nS>
38. Wang, D., Hwang, M., Jiang, W.C., Ding, K., Chang, H.C., Hwang, K.S.: A deep learning method for counting white blood cells in bone marrow images. *BMC bioinformatics* **22**(Suppl 5), 94 (2021)

39. Wang, W., Gao, Z., Gu, L., Pu, H., Cui, L., Wei, X., Liu, Z., Jing, L., Ye, S., Shao, J., et al.: Internvl3. 5: Advancing open-source multimodal models in versatility, reasoning, and efficiency. arXiv preprint arXiv:2508.18265 (2025)
40. Wei, J., Wang, X., Schuurmans, D., Bosma, M., Ichter, B., Xia, F., Chi, E., Le, Q.V., Zhou, D.: Chain-of-thought prompting elicits reasoning in large language models. In: Koyejo, S., Mohamed, S., Agarwal, A., Belgrave, D., Cho, K., Oh, A. (eds.) *Advances in Neural Information Processing Systems*. vol. 35, pp. 24824–24837. Curran Associates, Inc. (2022), [https://proceedings.neurips.cc/paper\\_files/paper/2022/file/9d5609613524ecf4f15af0f7b31abca4-Paper-Conference.pdf](https://proceedings.neurips.cc/paper_files/paper/2022/file/9d5609613524ecf4f15af0f7b31abca4-Paper-Conference.pdf)
41. Wies, N., Levine, Y., Shashua, A.: Sub-task decomposition enables learning in sequence to sequence tasks. In: *The Eleventh International Conference on Learning Representations (2023)*, <https://openreview.net/forum?id=BrJATVZDWEH>
42. Wu, Q., Yang, X., Zhou, Y., Fang, C., Song, B., Sun, X., Ji, R.: Grounded chain-of-thought for multimodal large language models. arXiv preprint arXiv:2503.12799 (2025)
43. Xia, J., Tong, B., Zang, Y., Shao, R., Zhou, K.: Bootstrapping grounded chain-of-thought in multimodal llms for data-efficient model adaptation. In: *Proceedings of the IEEE/CVF International Conference on Computer Vision (ICCV)*. pp. 208–217 (October 2025)
44. Xie, W., Noble, J.A., Zisserman, A.: Microscopy cell counting and detection with fully convolutional regression networks. *Computer methods in biomechanics and biomedical engineering: Imaging & Visualization* **6**(3), 283–292 (2018)
45. Yang, W., Huang, Z.: Poivre: Self-refining visual pointing with reinforcement learning. arXiv preprint arXiv:2509.23746 (2025)
46. Yi, K., Wu, J., Gan, C., Torralba, A., Kohli, P., Tenenbaum, J.: Neural-symbolic vqa: Disentangling reasoning from vision and language understanding. In: Bengio, S., Wallach, H., Larochelle, H., Grauman, K., Cesa-Bianchi, N., Garnett, R. (eds.) *Advances in Neural Information Processing Systems*. vol. 31. Curran Associates, Inc. (2018), [https://proceedings.neurips.cc/paper\\_files/paper/2018/file/5e388103a391daabe3de1d76a6739ccd-Paper.pdf](https://proceedings.neurips.cc/paper_files/paper/2018/file/5e388103a391daabe3de1d76a6739ccd-Paper.pdf)
47. You, Z., Yang, K., Luo, W., Lu, X., Cui, L., Le, X.: Few-shot object counting with similarity-aware feature enhancement. In: *Proceedings of the IEEE/CVF Winter Conference on Applications of Computer Vision*. pp. 6315–6324 (2023)
48. Yuan, W., Duan, J., Blukis, V., Pumacay, W., Krishna, R., Murali, A., Mousavian, A., Fox, D.: Robopoint: A vision-language model for spatial affordance prediction in robotics. In: *Conference on Robot Learning*. pp. 4005–4020. PMLR (2025)
49. Zhang, C., Wang, S.: Good at captioning bad at counting: Benchmarking gpt-4v on earth observation data. In: *Proceedings of the IEEE/CVF Conference on Computer Vision and Pattern Recognition*. pp. 7839–7849 (2024)
50. Zhang, H., Li, H., Li, F., Ren, T., Zou, X., Liu, S., Huang, S., Gao, J., Leizhang, Li, C., Yang, J.: Llava-grounding: Grounded visual chat with large multimodal models. In: Leonardis, A., Ricci, E., Roth, S., Russakovsky, O., Sattler, T., Varol, G. (eds.) *Computer Vision – ECCV 2024*. pp. 19–35. Springer Nature Switzerland, Cham (2025)
51. Zhou, D., Schärli, N., Hou, L., Wei, J., Scales, N., Wang, X., Schuurmans, D., Cui, C., Bousquet, O., Le, Q.V., Chi, E.H.: Least-to-most prompting enables complex reasoning in large language models. In: *The Eleventh International Conference on Learning Representations (2023)*, <https://openreview.net/forum?id=WZH7099tgfM>

## I Experimental Details

We complement the main paper by providing additional implementation details.

### A Models

We evaluate the following open-source LVLMs available on HuggingFace:

- Qwen2.5-VL 3B
- Qwen2.5-VL 7B
- LLaVA-OneVision-1.5 8B
- InternVL3.5 8B

These models were selected because they represent state-of-the-art open-source LVLMs with different architectural choices and image preprocessing strategies, as discussed in Sec. 3.4 of the main paper. In addition, we conduct preliminary experiments with Molmo-7B-O.

### B Training

We train each model using LoRA [16] (rank  $r = 32$ , scaling  $\alpha = 64$ ), inserting adapters into the query, key, and value matrices of LLM, vision encoder, and modality projection layer (when present). Models are loaded in FP16 precision and optimized using AdamW with default parameters and a learning rate of  $1 \times 10^{-5}$  (which achieved the lowest validation perplexity in preliminary experiments). Training runs for up to 10 epochs, with early stopping (patience = 2) based on validation perplexity. All experiments are conducted on a single NVIDIA A100 (80 GiB) GPU with batch size 1, and images are processed using each model’s default pre-processing pipeline. Under this configuration, each experiment requires at most two days.

### C Inference

During inference, answers are generated using greedy decoding with each LVLM’s default stopping criterion. To reduce verbose responses, we append the instruction “*Answer with as few words as possible*”, following prior findings [35]. We set `max_new_tokens = 5` for DC and `max_new_tokens = 1000` for PtC, ensuring that each model can produce the coordinates and the final answer regardless of differences across tokenizers.

To extract the predicted count  $\hat{y}$ , we apply a regular expression that first converts textual numbers into digits (e.g., “one”  $\rightarrow$  1, “five”  $\rightarrow$  5, “twenty”  $\rightarrow$  20) and then extracts the first consecutive sequence of digits from the generated output. If no valid number can be matched, we return  $-1$ . For PtC models, the same procedure is applied after locating the *Answer:* field. Predicted grounding coordinates are extracted using a separate regular expression that matches tuples of the form  $(n, m)$  in the generated output, while discarding malformed pairs. The predicted coordinate set is then evaluated against the ground-truth set  $\mathcal{C}$ .

## II Dataset Construction

As image size can affect model accuracy, we generate images at a resolution of  $672 \times 672$  pixels, following prior findings [35]. For models that do not support this resolution, we apply their default image pre-processing strategy.

As discussed in Sec. 3.2, we subdivide each image into a  $9 \times 9$  grid, where each cell corresponds to a  $74 \times 74$  pixel region. Since  $74 \times 9 = 666$ , we add 3 pixels of padding on each side so that the grid is centered within the  $672 \times 672$  image. Each object occupies an area of  $64 \times 64$  pixels and can be placed in the center of a cell. To avoid occlusions, we place each object in a distinct cell. Within the grid, coordinates are represented as tuples  $(n, m)$ , where  $n$  and  $m$  denote the row and column indices, respectively. The top-left cell corresponds to  $(0, 0)$ , while the bottom-right cell corresponds to  $(8, 8)$ .

Following prior work [3], we generate images incrementally to minimize differences between images containing  $i$  and  $i - 1$  target objects. Specifically, each image  $\mathcal{I}_i$  is obtained by adding one target object to  $\mathcal{I}_{i-1}$  (leaving the other objects unchanged). This ensures that consecutive images differ by exactly one object, allowing us to study how increasing the number of objects affects LVLMs while minimizing variation due to object position. We use the same procedure when introducing distractors into the scene.

Queries are generated using the template “How many *<color>* *<shape>*s are there?”, where the placeholders are replaced with the color and shape of the target object (e.g., “How many blue stars are there?”).

## III Preliminary Results

To ensure that the setting discussed in Secs. II and 3.2 does not induce a severe distribution shift, we run a preliminary experiment to assess the performance of LVLMs on the generated images. We report the prompts used to perform PtC in Figs. 5 and 6. For Molmo, we use a prompt closely aligned with the one reported in its corresponding paper [13]. For the other models, we evaluate three different prompts on a subset of the validation set and retain the one that achieves the best results. The results in Tab. 4 show that all pre-trained models achieve more than 66% accuracy (best results between DC and PtC) on the ID setting, suggesting that our images are compatible with their pre-training distribution. When asked to first point to the objects, Molmo’s performance almost doubles, reaching near-perfect accuracy and indicating that the model benefits considerably from point supervision. In contrast, the performance of Qwen2.5-VL 3B, LLaVA-OneVision, and InternVL3.5 decreases, suggesting that these models may not have been pre-trained to ground objects or to use such information for counting. The only exception is Qwen2.5-VL 7B, which achieves only a negligible gain in performance ( $< 2\%$ ). While this may indicate that the model was trained to use grounding as an intermediate subtask (as mentioned in its report [7]), the predicted coordinates do not follow the prompting schema and are, in most cases, out of bounds, making them unsuitable as visual explanations.

**Table 4:** Accuracy (%) of each pre-trained model under the ID setting when prompted to DC or PtC. Values in **bold** indicate the higher result between the two approaches. Overall, all models achieve more than 66% accuracy, suggesting that our images are compatible with their (pre-)training distribution. On PtC, only Molmo achieves near-perfect accuracy, while other models either degrade or show little change.

Model	DC	PtC
<i>Qwen2.5-VL 3B</i>	<b>66.79</b>	45.71
<i>Qwen2.5-VL 7B</i>	77.69	<b>78.42</b>
<i>LLaVA-OneVision 8B</i>	<b>87.20</b>	62.91
<i>InternVL3.5 8B</i>	<b>86.61</b>	77.42
<i>Molmo 7B</i>	53.06	<b>99.95</b>

Prompt template for PtC (Molmo)

Count by pointing.

**Fig. 5:** Prompt template used to perform PtC for Molmo.

Prompt template for PtC (others)

Count the object(s) in the image. First generate the object' location(s) (returning a pair of (x, y) coordinates between 0 and 100), then return the total number of objects. Only answer with \"Coordinates: ... Answer:\".

**Fig. 6:** Prompt template used to perform PtC for LLaVA-OneVision, InternVL3.5, and Qwen2.5-VL models.

## IV Additional Results & Analyses

We complement the main paper by providing additional results and analyses.

### A Compositional Generalization

We evaluate compositional generalization across object attributes by training the model on all individual shapes and colors while holding out specific shape-color combinations. At test time, the model is evaluated on these unseen combinations. Tabs. 5 and 6 report the average accuracy with the standard deviation across models in the ID setting for DC and PtC, respectively. Overall, PtC yields stronger compositional generalization, with two unseen shape-color combinations reaching 100% accuracy. PtC also exhibits lower variability across object types, with *blue squares* being the most challenging case while still achieving 99.59%

accuracy. By contrast, models fine-tuned with DC reach at most 99.69% accuracy, down to 93.90%, and are more sensitive to variations in shape and color. For instance, performance on *Squares* differs by roughly 3 percentage points between *red* and *magenta*. DC also exhibits greater variability across models, with *magenta squares* showing the largest standard deviation at 8.12 percentage points. In contrast, PtC exhibits at most a variability of 0.4 percentage points, suggesting better transferability across models. Finally, we show in Tab. 7 that *blue stars* is the color-shape combination with the highest accuracy and lowest standard deviation across models and training approaches. This motivates our choice of *blue stars* as the target object for the Noisy<sub>TS</sub> setting (Sec. 3.2).

Overall, our findings suggest that PtC promotes stronger compositional generalization across object types than DC.

**Table 5:** Accuracy (%) across object shape and color combinations on the ID setting for DC Models. Values report mean accuracy with standard deviation across models. Results in **bold** indicate the color-shape combination(s) with the highest accuracy and lower standard deviation.

	<i>Circles</i>	<i>Squares</i>	<i>Triangles</i>	<i>Stars</i>
<i>Red</i>	98.87 ± 1.06	96.85 ± 4.10	96.06 ± 7.61	99.31 ± 0.60
<i>Green</i>	99.01 ± 1.18	95.58 ± 5.68	96.71 ± 5.88	98.94 ± 1.61
<i>Blue</i>	<b>99.69 ± 0.62</b>	96.26 ± 4.20	97.46 ± 4.04	99.66 ± 0.24
<i>Cyan</i>	99.38 ± 0.69	95.71 ± 6.71	96.40 ± 6.66	99.25 ± 1.25
<i>Magenta</i>	99.14 ± 0.76	93.90 ± 8.12	95.03 ± 7.47	99.35 ± 0.49
<i>Yellow</i>	99.01 ± 0.70	96.50 ± 4.80	97.67 ± 4.39	98.80 ± 1.86

**Table 6:** Accuracy (%) across object shape and color combinations on the ID setting for PtC Models. Values report mean accuracy with standard deviation across models. Results in **bold** indicate the color-shape combination(s) with the highest accuracy and lower standard deviation.

	<i>Circles</i>	<i>Squares</i>	<i>Triangles</i>	<i>Stars</i>
<i>Red</i>	99.86 ± 0.11	99.83 ± 0.34	99.97 ± 0.07	99.93 ± 0.08
<i>Green</i>	99.90 ± 0.07	99.83 ± 0.21	99.93 ± 0.14	<b>100.00 ± 0.00</b>
<i>Blue</i>	99.86 ± 0.11	99.59 ± 0.40	99.93 ± 0.08	99.93 ± 0.08
<i>Cyan</i>	99.90 ± 0.07	99.86 ± 0.19	99.97 ± 0.07	99.97 ± 0.07
<i>Magenta</i>	99.97 ± 0.07	99.66 ± 0.29	99.97 ± 0.07	99.97 ± 0.07
<i>Yellow</i>	99.90 ± 0.07	99.79 ± 0.26	<b>100.00 ± 0.00</b>	99.97 ± 0.07

**Table 7:** Accuracy (%) across object shape and color combinations on the ID setting averaged across models and training approaches. Values report mean accuracy with standard deviation across models. Results in **bold** indicate the color-shape combination(s) with the highest accuracy and lower standard deviation.

	<i>Circles</i>	<i>Squares</i>	<i>Triangles</i>	<i>Stars</i>
<i>Red</i>	99.37 ± 0.88	98.34 ± 3.13	98.01 ± 5.41	99.62 ± 0.52
<i>Green</i>	99.45 ± 0.91	97.70 ± 4.36	98.32 ± 4.22	99.47 ± 1.19
<i>Blue</i>	99.78 ± 0.42	97.93 ± 3.29	98.70 ± 2.95	<b>99.79 ± 0.22</b>
<i>Cyan</i>	99.64 ± 0.53	97.79 ± 4.92	98.18 ± 4.76	99.61 ± 0.91
<i>Magenta</i>	99.55 ± 0.67	96.78 ± 6.14	97.50 ± 5.55	99.66 ± 0.46
<i>Yellow</i>	99.45 ± 0.66	98.15 ± 3.61	98.83 ± 3.13	99.38 ± 1.37

## B Grounding

We complement the main paper by reporting cell-level F1-scores for the remaining settings. As expected from Tab. 2, most models achieve high and spatially consistent F1-scores across the entire image in the ID setting, as illustrated in Fig. 7. The only exception is LLaVA-OneVision, which shows slightly reduced grounding performance near the image boundaries. Figure 8 presents the corresponding results for the OOD setting. Most LVLMs exhibit the same spatial biases observed in Fig. 4. The main exception is Qwen2.5-VL 3B, which appears to struggle more in this setting, with lower F1-scores in the central region of the image.



**Fig. 7:** Cell-level F1-score (%) for each model across our  $9 \times 9$  grid on the ID setting.

Since some models may occasionally produce coordinates that fall outside the image boundaries, which would lower the F1-score for specific spatial regions, we report the percentage of out-of-bounds predictions for each setting in Tab. 8. Overall, such errors are extremely rare, occurring in fewer than 0.21% of the cases across all models and settings. In particular, Qwen2.5-VL 3B and InternVL3.5 never produce out-of-bounds coordinates in any setting, while the remaining models only exhibit negligible rates. Interestingly, these errors appear almost exclusively in the more challenging OOD and Noisy<sub>T5</sub> settings, sug-

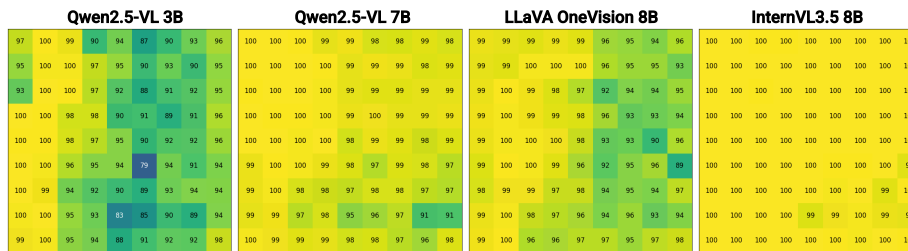


**Fig. 8:** Cell-level F1-score (%) for each model across our  $9 \times 9$  grid on the OOD setting.

gesting that distribution shifts and the presence of distractors slightly increase the likelihood of invalid coordinate predictions. Among the evaluated models, LLaVA-OneVision shows the highest out-of-bounds rate, although it remains below 0.21%.

Overall, these results indicate that invalid coordinate predictions are not a significant source of error in our evaluation, validating the grounding trends reported in Figs. 4, 7 and 8 and confirming that the variations in F1-score primarily reflect the presence of spatial biases.

**Table 8:** Percentage (%) of out-of-bounds coordinates predicted by each model across the ID, OOD, and `NoisyTS` settings. Results for `NoisyTS` are computed only on images containing 9 distractors.

Model	ID	OOD	Noisy <sub>TS</sub>
<i>Qwen2.5-VL 3B</i>	0.00	0.00	0.00
<i>Qwen2.5-VL 7B</i>	0.00	0.09	0.03
<i>LLaVA-OneVision 8B</i>	0.01	0.08	0.20
<i>InternVL3.5 8B</i>	0.00	0.00	0.00

### C Performance of X Fine-Tuning on the ID setting

To show that models fine-tuned to output “X” tokens instead of coordinates can still count accurately on in-distribution examples, yet fail to generalize to object counts beyond those observed during fine-tuning (as shown in Tab. 3a), we evaluate them on the ID setting. The results in Tab. 9 show that, although models fine-tuned to output “X” instead of coordinates exhibit slightly lower performance than their PtC counterparts (< 3%), all models still achieve more than 97% accuracy. This suggests that, in the ID setting, models can rely on coarse visual cues or on the textual pattern learned during fine-tuning to solve the task even without explicit spatial grounding. However, their accuracy drops substantially on the OOD setting, as shown in Tab. 3a. Taken together, these

results indicate that replacing spatial information with a generic token preserves in-distribution performance, but removes the explicit grounding signal required to generalize to higher object counts. This further supports our main claim that spatial supervision is a key factor underlying the improved extrapolation ability of PtC.

**Table 9:** Accuracy (%) of each model on the ID setting after X Fine-Tuning, where each coordinate is replaced with an “X” during PtC training. Values in parentheses indicate the absolute change with respect to the corresponding PtC baseline.

<b>Model</b>	<b>X Fine-Tuning</b>
<i>Qwen2.5-VL 3B</i>	98.11 (↓ 1.83)
<i>Qwen2.5-VL 7B</i>	97.37 (↓ 2.51)
<i>LLaVA-OneVision 8B</i>	99.71 (↓ 0.05)
<i>InternVL3.5 8B</i>	99.87 (↓ 0.13)